CHAPTER 4
EFFECT OF BORON AND NITROGEN DOPING ON MOLECULAR ADSORPTION

4.1. INTRODUCTION

Carbon allotropes, including diamond and graphite, have diverse physical, chemical, electronic, and reactive properties [1]. These materials are widely used in various domains, such as energy storage, optoelectronics, catalysis, medicine, and gas separation and sensing. Kaiser et al. successfully synthesized cyclo[18]carbon (C_{18}), the smallest all-carbon electron acceptor, in 2019 [2], which has received significant attention for its excellent sensing properties. Researchers have been working on developing carbon-based sensors that are cost-effective and sensitive to certain gases due to the lethality of these poisonous gases on living organisms. Carbon nanostructures such as C_{60}, graphene, graphene nanoribbons, carbon dots (GQD), and nanotubes (CNT) have been investigated for gas sensing applications [3]. Other carbon-based materials, such as carbon oxide quantum dots, boron nitride nanotubes (BNNT), and boron nitride nanosheets (BNNS), have also been used for gas sensing applications [4-5].

Literature surveys reveal that the HOMO-LUMO gap of pristine C_{18} nanocluster is 6.74 eV, indicating poor conductivity [6]. To improve its conducting characteristics, impurity doping is required. Since boron and nitrogen atoms are almost of the same sizes as carbon atoms, they can easily substitute themselves in lieu of some of the host atoms in the nanocluster [7], producing a substitutional impurity without causing distortion to the original cluster. The adsorption performances of CO, NO, and NH_3 gases on doped polyynic C_{18} nanoclusters have been performed in this study. The density functional theory based on first-principles calculations was used to analyze the structural, electronic, and adsorption properties of all adsorbed systems. Doping (B and N) is a good way to tune the fundamental properties of polyynic and its adsorption performance towards the aforementioned gases.

The aim is to examine the sensing performance of $C_{17}B$, $C_{17}N$ nanoclusters towards CO, NO, and NH_3 gases to find out whether they show any improvement compared to the pristine C_{18} nanocluster. The findings of this chapter will be useful not only in synthesizing low-cost, very sensitive C_{18} sensors for detecting hazardous gases but also in understanding how these systems interact on the surface with said gases.

4.2. METHODOLOGY

The study utilizes Gaussian 09 package [8] for first principles-based structural calculations on $C_{17}X$ nanoclusters. The hybrid ωB97XD is used to computationally replicate the experimentally synthesized structural geometry of C_{18} nanocluster [9]. The calculations are performed using the 6-311++G(d, p) basis set and are adapted to compute energies, electronic

properties, global indices, and recovery time. Images of molecular structures and Mulliken charges are obtained from GaussView 6.0 using first principles calculations. The density of states spectra are obtained using GaussSum 3.0. The separation from highest occupied molecular orbital to lowest unoccupied molecular orbital in terms of energy is given by [10]:

$$E_G = E_{LUMO} - E_{HOMO} \text{ ---- (1)}$$

The energy value at the Fermi level (E_F) is [11]:

$$E_F = (E_{LUMO} + E_{HOMO})/2 \text{ ---- (2)}$$

4.3. RESULTS AND DISCUSSION

4.3.1. Physical and Electronic Characteristics of B, N doped C_{18} Nanoclusters

Before delving into the adsorption investigation, the $C_{17}B$ and $C_{17}N$ underwent geometry optimization. The illustration in Figure 4.1 portrays the optimized configuration of C_{18} nanoclusters doped with B and N. In the case of $C_{17}B$, the calculated lengths for C-C and C ≡ C bonds are 1.33 Å and 1.23 Å, respectively, while the C-B bond registers a length of 1.43 Å. The average angle among C-C-C atoms stands at 157.64 degrees, while the angle undergoes a shift to 163.66 degrees following B-doping (C_1-B-C_{17}), illustrated in Fig. 4.1(a). In the case of $C_{17}N$, the optimized lengths for C-C and C ≡ C bonds are 1.33 Å and 1.23 Å, respectively, with the C-N bond length measuring 1.3 Å. The average angle formed by C-C-C atoms is 159.76 degrees, and post N-doping (C_1-N-C_{17}), the angle adjusts to 117.35 degrees, as depicted in Fig. 4.1(b).

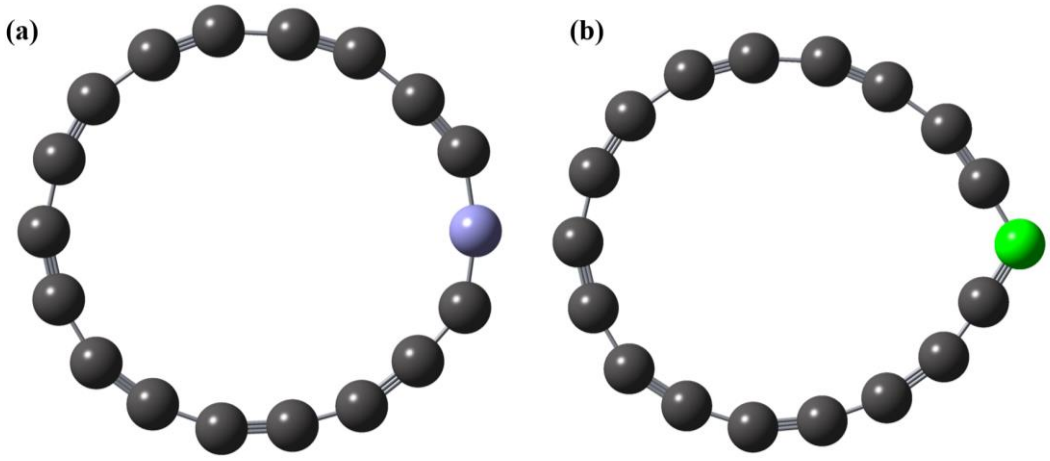

Figure 4.1: optimized geometries of (a) $C_{17}B$ nanocluster (b) $C_{17}N$ nanocluster

:

Following the doping process, the molecular orbitals experience a doublet splitting, giving rise to α and β orbitals (representing spins up and down). The energy values for occupied and unoccupied orbitals are as follows: -7.93 eV(α), -7.45 eV(β) and -1.78 eV(α), -2.08 eV(β), respectively. The calculated energy gap (E_G) for the $C_{17}B$ nanocluster, using equation (1), is 6.15 eV(α) and 4.14 eV(β). As for the $C_{17}N$ nanocluster, the E_{HOMO} and E_{LUMO} values are -7.68 eV(α), -8.51 eV(β) and -2.95 eV(α), -2.55 eV(β), respectively. The resulting E_G is 4.73 eV(α) (or 5.96 eV(β)), notably lower than the original [6, 9].

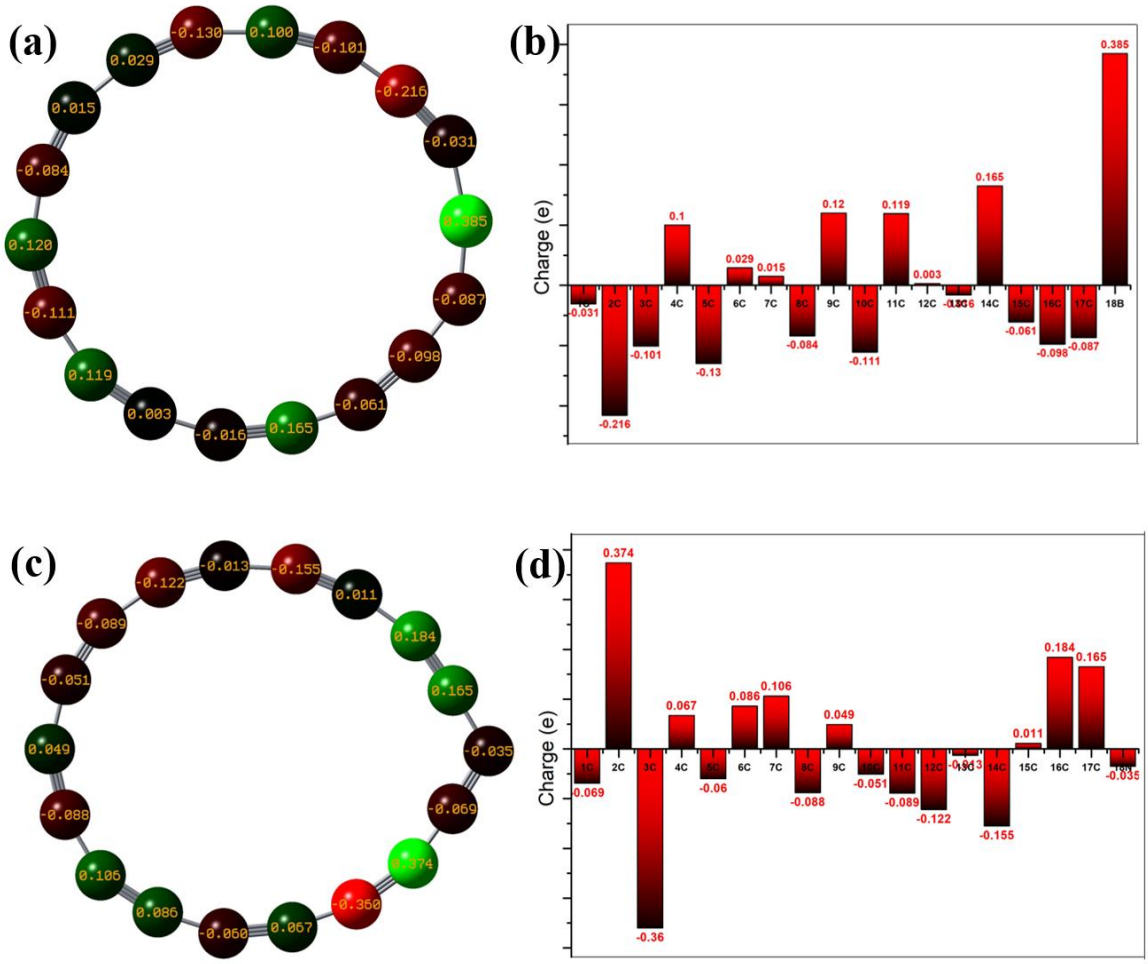

Figure 4.2: (a, b) Mulliken charge population and Mulliken plot of (a, b) $C_{17}B$ and (c,d) $C_{17}N$ nanocluster

The E_F values stand at -5.30 eV and -4.84 eV for $C_{17}B$ and $C_{17}N$, respectively. Computed using equation (2), these values reside in the midpoint between the HOMO and LUMO. Our examination involved the Mulliken atomic charge distribution, illustrating the positive and negative charge distribution across each carbon and impurity atom (refer to Fig. 4.2(a, b, c, and d)). Additionally, Fig. 4.3(a) and 4.3(b) showcase density of states (DOS) plots for the $C_{17}B$

and $C_{17}N$ nanoclusters, providing support for the calculated E_{HOMO}, E_{LUMO}, and E_G values as outlined in Table 4.1. To verify the stability of $C_{17}X$ nanoclusters, where X represents either B or N, the calculation of formation energies (E_{form}) was performed as outlined [12]:

$$E_{form} = [E(C_{17}X)-17\cdot E(C)-E(X)]/18 \text{ ----- (3)}$$

In this context, $E(C_{17}X)$ represents the ground state energy of the $C_{17}X$ nanocluster, E(C) is the energy of an isolated carbon atom, and E(X) denotes the energy of a single boron or nitrogen atom. The computed formation energy values are -7.73 eV/atom for $C_{17}B$ and -7.83 eV/atom for $C_{17}N$ nanocluster. The negative signs associated with the formation energies signify the stability of these structures [13].

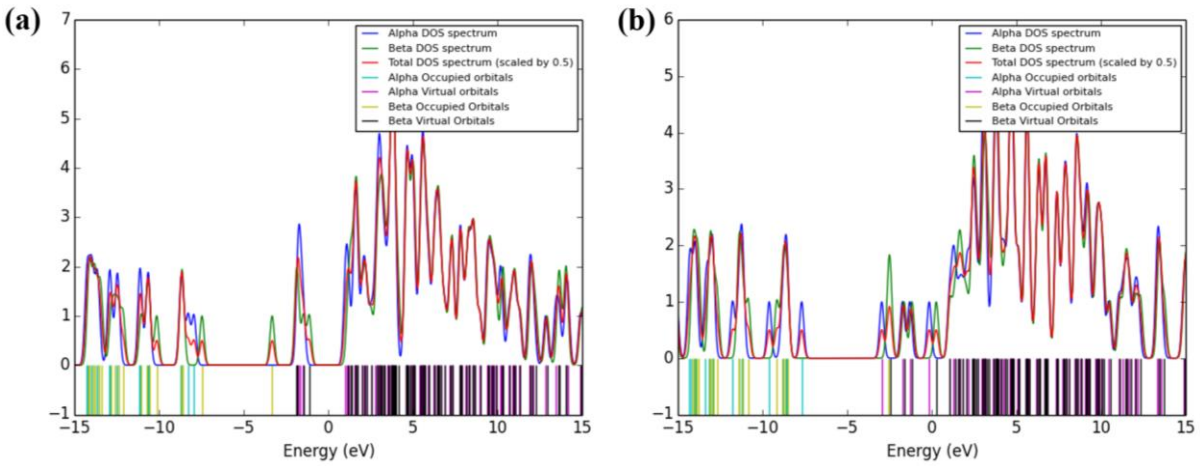

Figure 4.3: DOS plots for (a) $C_{17}B$ nanocluster (b) $C_{17}N$ nanocluster

Table 4.1: Bond length and Angle, E_{HOMO} and E_{LUMO}, and E_G for $C_{17}X$ nanoclusters.

System	Bond length (Å)		Angle (°)		E_{HOMO} (eV)	E_{LUMO} (eV)	E_G (eV)	E_F (eV)
	C-C	C≡C	θ_1	θ_2				
$C_{17}B$	1.33	1.23	159.76°	117.35°	$-7.93^{(\alpha)}$ $-7.45^{(\beta)}$	$-1.78^{(\alpha)}$ $-3.31^{(\beta)}$	$6.15^{(\alpha)}$ $4.14^{(\beta)}$	$-4.86^{(\alpha)}$ $-5.38^{(\beta)}$
$C_{17}N$	1.33	1.23	157.64°	163.66°	$-7.68^{(\alpha)}$ $-8.51^{(\beta)}$	$-2.95^{(\alpha)}$ $-2.55^{(\beta)}$	$4.73^{(\alpha)}$ $5.96^{(\beta)}$	$-5.32^{(\alpha)}$ $-5.53^{(\beta)}$

4.3.2. Adsorption study of CO, NO and NH_3 gas molecules over $C_{17}X$ nanoclusters

The analysis of the interaction between gas molecules and $C_{17}X$ nanoclusters, where X represents either B or N, is conducted through adsorption energy, employing the following equation [14]:

$$E_{ad} = E(C_{17}X+Gas) – E(C_{17}X) - E(Gas) \text{ ---- (4)}$$

In this context, $E(C_{17}X+gas)$, $E(C_{17}X)$, and E(gas) represent the total energy of the gas-adsorbed $C_{17}X$ nanocluster, the total energy of the $C_{17}X$ ring, and the total energy of an individual gas molecule, respectively. Specifically for CO and NO molecules, we deliberately selected diverse adsorption sites on $C_{17}X$ nanoclusters (such as above carbon and impurity atoms, over C-C and C ≡ C bonds) and explored various orientations of gas molecules (with C, N, or O as the head for CO and NO), ensuring a comprehensive analysis at each site. Conversely, we opted for N head, H head, and a horizontal orientation when considering NH_3 molecules. From the numerous configurations examined, those displaying the lowest energies were singled out for subsequent calculations.

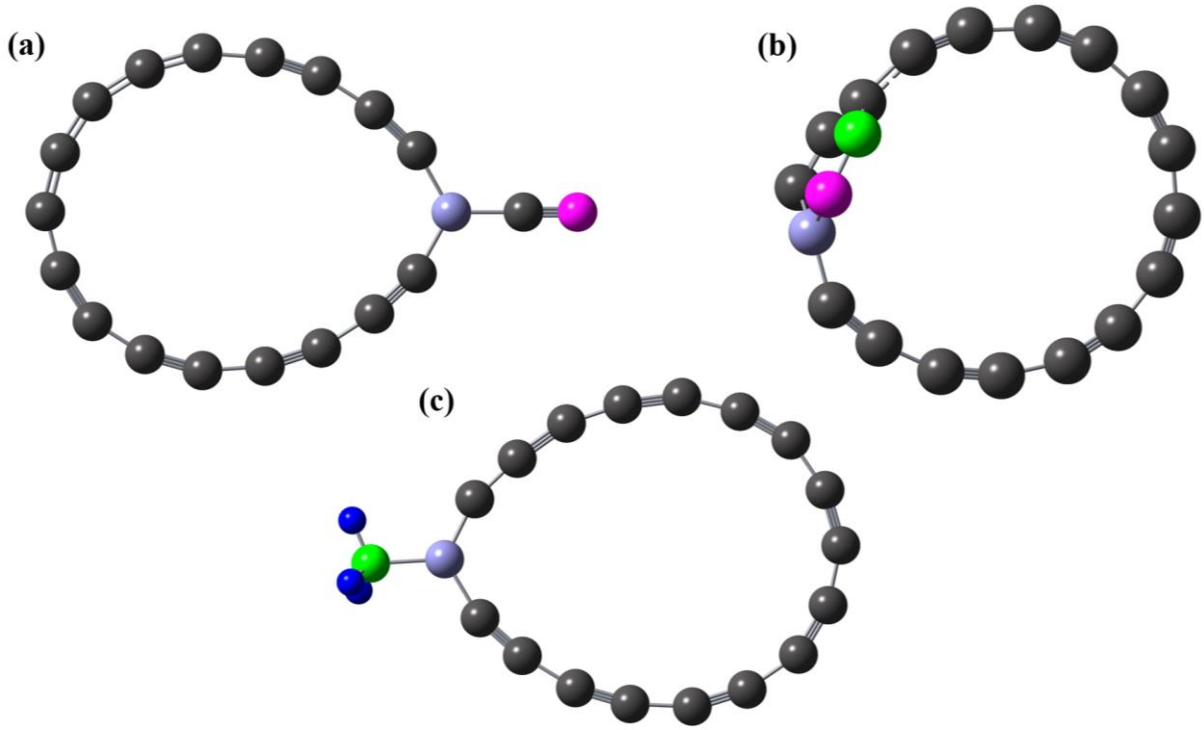

Figure 4.4: Lowest energy configurations of (a) CO (b) NO (c) NH_3 adsorbed $C_{17}N$ nanocluster

The computed adsorption energy (E_{ad}) for carbon monoxide over the $C_{17}B$ nanocluster is -1.41 eV, as determined by equation (4). In Fig. 4.4(a), the most stable configuration post-adsorption is depicted. The adsorption distance for the carbon atom of CO gas is 1.51 Å from the dopant B atom of the $C_{17}B$ nanocluster. Similarly, for NO and NH_3 adsorption, the lowest energy configurations are illustrated in Fig. 4(b, c), with E_{ad} values of -2.00 eV for NO and -1.87 eV for NH_3 adsorption. Following the adsorption of nitric oxide, the nitrogen atom of the NO gas molecule is positioned at a distance of 1.42 Å from the adjacent atom of the $C_{17}B$ nanocluster (refer to Fig. 4.4(b)). Conversely, post-NH_3 adsorption, the distance between the

N head of the NH_3 molecule and the dopant B atom of the $C_{17}B$ is 1.59 Å (see Fig. 4.4(c)). The short adsorption distances coupled with more negative adsorption energies strongly indicate the chemisorptive nature of CO, NO, and NH_3 towards the $C_{17}B$ nanocluster.

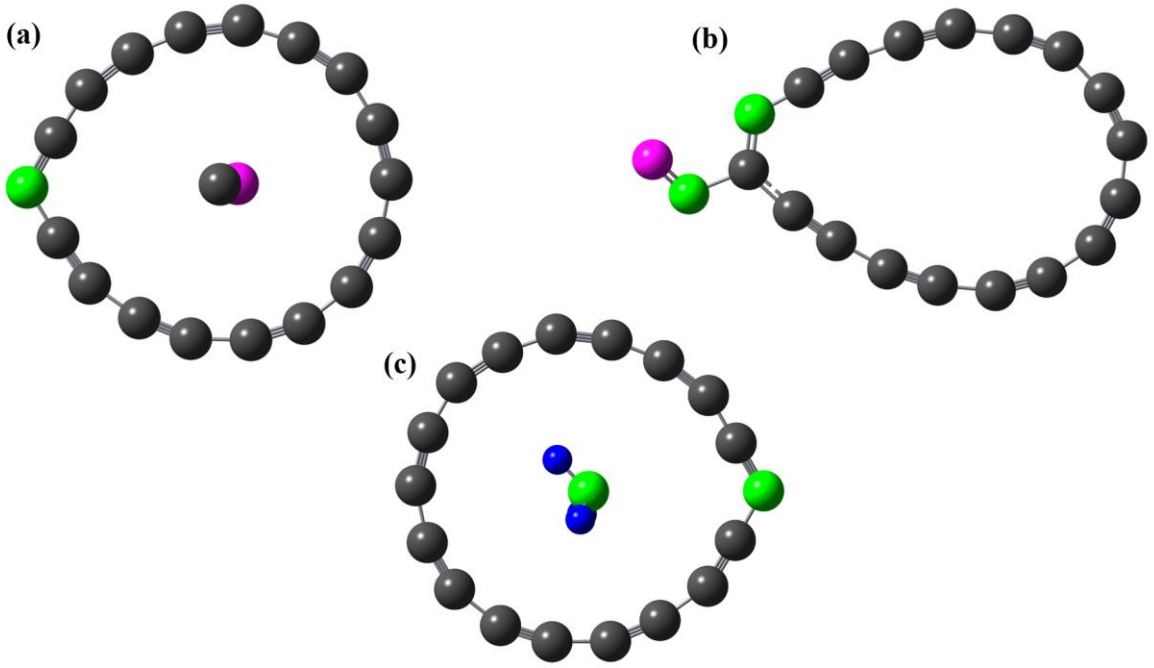

Figure 4.5: Lowest energy configurations of (a) CO (b) NO (c) NH_3 adsorbed $C_{17}N$ nanocluster

Carbon monoxide has an adsorption energy of -0.15 eV over the $C_{17}N$ nanocluster. The lowest energy conformer of the gas molecule following CO adsorption occurs in the hollow of the $C_{17}N$ nanocluster, as seen in Fig. 4.5(a). The determined adsorption distance is 4.28 Å. Likewise, for NH_3 adsorption, Fig. 4.5(c) illustrates the configurations with the lowest energy. The computed adsorption energy (E_{ad}) is -0.25 eV, and the corresponding adsorption distance (d) measures 3.41 Å. The computed E_{ad} is -1.32 eV after nitric oxide adsorption, whereas the d is 1.49 Å (see Fig 4.5(b)). The gas molecules CO and NH_3 show physisorption towards the $C_{17}N$ nanocluster, whereas NO shows chemisorption, according to the values of the adsorption energies.

4.3.3. Electronic properties of CO, NO and NH_3 adsorbed $C_{17}X$ nanoclusters

As a result of the molecules of gases adhering to the nanoclusters, there is a charge transfer [15]. After NH_3, CO, and NO have been adsorbed, the total Mulliken charge on the gas molecules is +0.521e, +0.016e, and +0.170e, respectively. This shows that since each gas molecule has a net zero charge, the charge is moving from the $C_{17}B$ nanocluster to the CO, NO, and NH_3 gas molecules. The Mulliken plots and the charge distribution of the gas adsorbed

$C_{17}B$ nanocluster are displayed in Figure 4.6(a, b, c, d, e, and f). After CO, NO, and NH_3 adsorption, the Mulliken charges on the gas molecules in the $C_{17}N$ nanocluster are -0.008e, +0.020e, and -0.144e, respectively. It suggests that, in the case of CO and NH_3 gas molecules, charge is moving from the gas molecule to the $C_{17}N$ nanocluster [16]. On the other hand, in NO gas, the charge is moving from the $C_{17}N$ nanocluster to the gas molecule. The Mulliken plots and the charge population of the gas adsorbed $C_{17}N$ nanocluster are displayed in Figure 7(a, b, c, d, e, and f). Additionally, the energies of E_G, ΔE_G, E_F, HOMO, LUMO, and ΔE_F have been computed and are shown in Table 4.2.

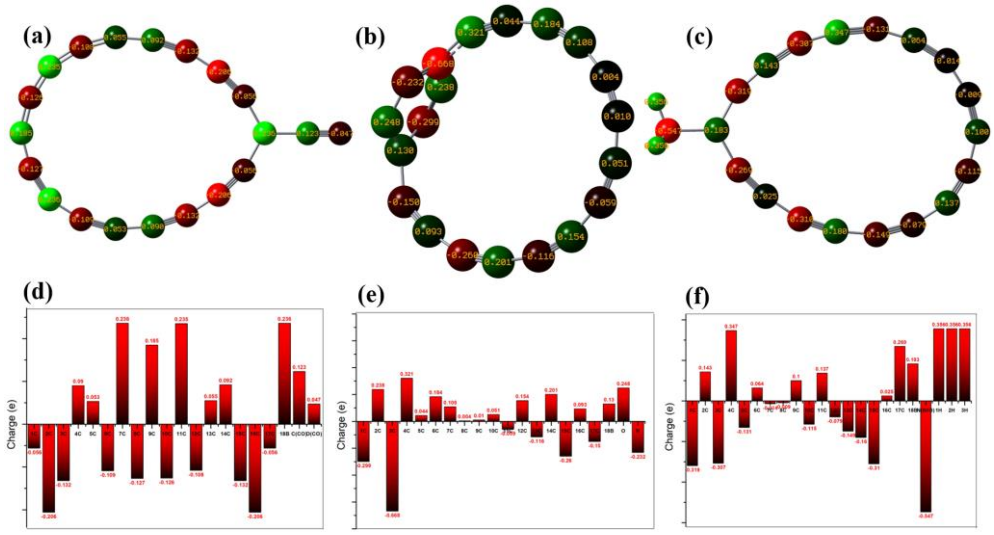

Figure 4.6: (a, b, c) Mulliken charge distributions (d, e, f) Mulliken plots of CO, NO and NH_3 adsorbed $C_{17}B$ nanocluster, respectively

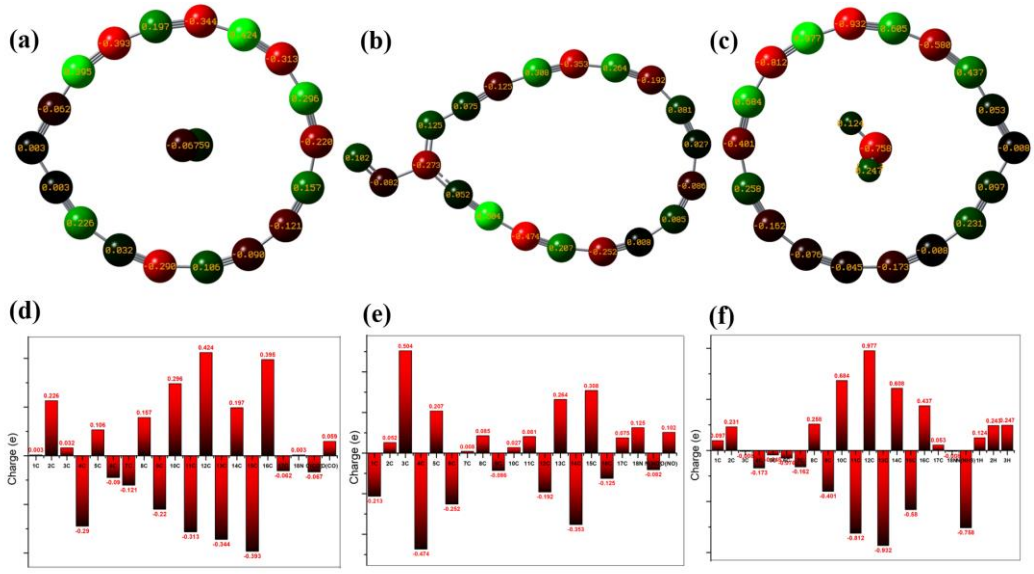

Figure 4.7: (a, b, c) Mulliken charge populations (d, e, f) Mulliken plots of CO, NO and NH_3 adsorbed $C_{17}N$ nanocluster, respectively

Table 4.2: E_{ad}, E_{HOMO} and E_{LUMO}, E_F and corresponding shift (δE_F), E_G and its relative change (ΔE_G), work function (φ), change in work function ($\Delta\varphi$) and adsorption distance (d) of CO, NO and NH_3 adsorbed $C_{17}X$ (X=B,N) nanoclusters, respectively.

System	E_{ad} (eV)	E_{HOMO} (eV)	E_{LUMO} (eV)	E_F (eV)	δE_F (eV)	E_G (eV)	ΔE_G	φ (eV)	$\Delta\varphi$	d (Å)
$CO/C_{17}B$	-1.41	$-7.49^{(\alpha)}$ $-7.23^{(\beta)}$	$-3.27^{(\alpha)}$ $-3.00^{(\beta)}$	$-5.38^{(\alpha)}$ $-5.12^{(\beta)}$	$-0.52^{(\alpha)}$ $+0.26^{(\beta)}$	$4.22^{(\alpha)}$ $4.23^{(\beta)}$	$-31.4\%^{(\alpha)}$ $2.17\%^{(\beta)}$	$5.38^{(\alpha)}$ $5.12^{(\beta)}$	$10.7\%^{(\alpha)}$ $-4.83\%^{(\beta)}$	1.51
$NO/C_{17}B$	-2.00	-7.95	-3.41	-5.68	-0.82	4.54	-26.2%	5.68	16.9%	1.42
$NH_3/C_{17}B$	-1.81	$-7.22^{(\alpha)}$ $-6.69^{(\beta)}$	$-0.97^{(\alpha)}$ $-2.08^{(\beta)}$	$-4.09^{(\alpha)}$ $-4.39^{(\beta)}$	$+0.77^{(\alpha)}$ $+0.99^{(\beta)}$	$6.25^{(\alpha)}$ $4.61^{(\beta)}$	$1.63\%^{(\alpha)}$ $11.4\%^{(\beta)}$	$4.09^{(\alpha)}$ $4.39^{(\beta)}$	$-15.8\%^{(\alpha)}$ $-18.4\%^{(\beta)}$	1.59
$CO/C_{17}N$	-0.15	$-7.71^{(\alpha)}$ $-8.57^{(\beta)}$	$-2.98^{(\alpha)}$ $-2.59^{(\beta)}$	$-5.35^{(\alpha)}$ $-5.58^{(\beta)}$	$-0.03^{(\alpha)}$ $-0.05^{(\beta)}$	$4.73^{(\alpha)}$ $5.98^{(\beta)}$	$0\%^{(\alpha)}$ $0.34\%^{(\beta)}$	$5.35^{(\alpha)}$ $5.58^{(\beta)}$	$0.56\%^{(\alpha)}$ $0.90\%^{(\beta)}$	4.28
$NO/C_{17}N$	-1.32	-8.44	-3.01	-5.73	-0.41	5.43	14.8%	5.73	7.71%	1.49
$NH_3/C_{17}N$	-0.25	$-7.56^{(\alpha)}$ $-8.50^{(\beta)}$	$-2.81^{(\alpha)}$ $-2.48^{(\beta)}$	$-5.19^{(\alpha)}$ $-5.49^{(\beta)}$	$+0.13^{(\alpha)}$ $+0.04^{(\beta)}$	$4.75^{(\alpha)}$ $6.02^{(\beta)}$	$0.42\%^{(\alpha)}$ $1.01\%^{(\beta)}$	$5.19^{(\alpha)}$ $5.49^{(\beta)}$	$-2.44\%^{(\alpha)}$ $-0.72\%^{(\beta)}$	3.41

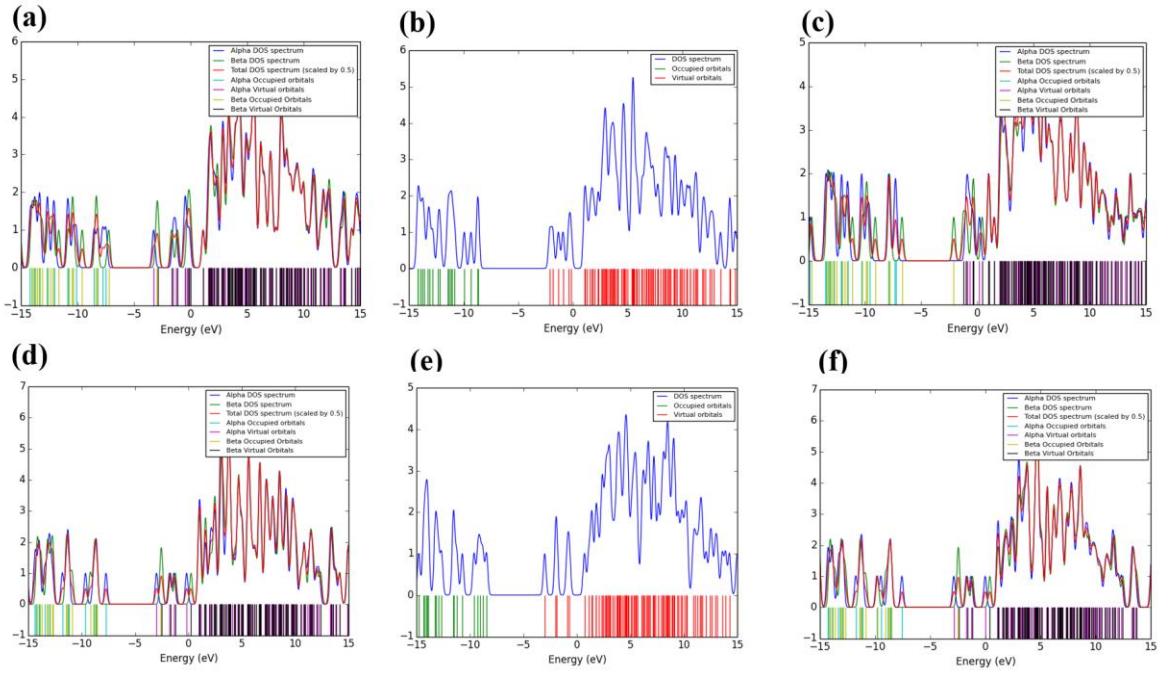

Figure 4.8: DOS plots for CO, NO and NH_3 adsorbed (a, b, c) $C_{17}B$ nanocluster (d, e, f) $C_{17}N$ nanocluster, respectively

As shown in Fig. 4.8(a, b, c, d, e, and f)), we have examined the density of states for gas molecules adsorbed $C_{17}X$ nanoclusters and compared it with the $C_{17}B$ and $C_{17}N$ nanoclusters. In comparison to the C17B nanocluster, following CO adsorption, E_G reduces by 31.4%(α) (or increases by 2.17%(β)), and the Fermi level changes down by 0.52 eV(α) (or up

by 0.26 eV(β)), which is consistent with the interpretation of the DOS plot. The shifting of the associated Fermi level and the change in E_F are indicated by table 4.2 and the density of states graphs. E_G falls by 26.2% in relation to the $C_{17}B$ nanocluster following the NO adsorption. The NH_3 adsorption also results in a rise of 1.63%(α) (or 11.6%(β)) in the energy gap (E_G), whereas the Fermi level decreases by 0.82 eV. The DOS charts provide confirmation for the E_G increases and Fermi level displacement. In contrast to the initial 4.73 eV(α) (or 5.96 eV(β)), the HOMO-LUMO energy gap either remains unchanged (α) or slightly rises (β) following the interaction of the CO molecule with the $C_{17}N$ nanocluster. Regarding the Fermi level shift, it decreases by 0.03 eV(α) (or by 0.05 eV(β)). Following the NO adsorption, E_F moves down by 0.41 eV and E_G rises by 14.8%. On the other hand, following NH_3 adsorption, the Fermi level rises by 0.13 eV(α) (or by 0.04 eV(β)) and the energy gap increases by 0.42%(α) (or 1.01%(β)). Table 4.2 confirms the growth and decrease in energy gaps and the shifting of the Fermi level. The figure's DOS charts support the changes in the electrical characteristics as well. The accompanying documentation (see s3) has a thorough explanation of work function.

4.3.4. Sensing properties of $C_{17}X$ nanoclusters

The sensing capabilities of $C_{17}X$ nanoclusters towards certain gas molecules are uncovered by an analysis of their electrical conductivity [17].

$$\sigma \propto \exp\left(-\frac{E_G}{2KT}\right) \text{ ----- (5)}$$

where T is the temperature, K is Boltzmann's constant, E_G, and σ is electrical conductivity. According to equation (5), conductivity increases as the E_G narrows because it varies inversely with respect to the band gap at a given temperature. Refer to Table 4.2. Because of their drop in E_G, the $C_{17}X$ nanoclusters exhibit a significant increase in conductivity when exposed to CO, NO, and NH_3. As E_G narrows, the $C_{17}X$ nanocluster's resistivity decreases. The resistance of the material is influenced by the concentration of gas molecules in the surrounding air in a proportional way. Effective gas-molecule interaction modifies the electronic properties of the $C_{17}X$ nanocluster significantly, indicating that it might be employed as an electronic sensor for gas-molecule detection. The E_G of the $C_{17}B$ nanocluster reduces by 31.4%(α) upon CO adsorption, indicating a sharp drop in electrical conductivity and, as a result, a significant sensing response. In E_G, CO(-31.4%(α)/2.17%(β)) > NO(-26.2%) > NH_3(1.63%(α)/11.4%(β)) is the order of decrease for $C_{17}B$. On the other hand, for $C_{17}N$, the decrement order is CO(0%(α)/0.34%(β) > NH_3(0.42(α)/11.4%(β)) > NO(14.8%).

For gas sensors, recovery time (τ) is an additional important component. It may be defined as the expected time interval prior to the adsorbate self-desorbing. Stated differently, recovery time determines how simple or complex the desorption process is. A quicker recovery time is what one would like in a sensor. A strong contact between a gas sensor and the gases should be avoided since this would prolong the recovery time of the sensor and make it more difficult for the gas molecules to separate provides τ [18].

$$\tau = \upsilon^{-1} \exp\left(-\frac{E_{ad}}{KT}\right) \text{----- (6)}$$

We used the attempt frequency υ = 1012 s-1 (for infrared radiation) and the absolute temperature T = 300 K to determine τ (see table 4.3).

Table 4.3: Calculated recovery time of CO, NO and NH_3 adsorbed $C_{17}B$, $C_{17}N$ nanoclusters for T = 300 K, υ = 10^{12} s^{-1}

System	$CO/C_{17}B$	$NO/C_{17}B$	$NH_3/C_{17}B$	$CO/C_{17}N$	$NO/C_{17}N$	$NH_3/C_{17}N$
Recovery Time	5×10^{11} s	4×10^{21} s	2.5×10^{16} s	0.33 ns	2×10^{10} s	14.8ns

4.3.5. Quantum Chemical Descriptors

The reactivity of the nanoclusters or quantum materials is determined using quantum chemical descriptors such as chemical potential (μ), softness (S), hardness (η), and electrophilicity (ω). They come from [19]:

$$\text{Chemical potential } (\mu) = -\frac{\text{I+A}}{2} \text{ --- (8)}$$

$$\text{Hardness } (\eta) = \frac{\text{I−A}}{2} \text{ --- (9)}$$

$$\text{Softness (S)} = \frac{1}{2\eta} \text{ --- (10)}$$

$$\text{Electrophilicity } (\omega) = \frac{\mu^2}{2\eta} \text{ --- (11)}$$

where $I \cong -E_{HOMO}$ and $A \cong -E_{LUMO}$.

In contrast to the $C_{17}N$ nanocluster, which has chemical potentials of -5.31 eV(α) and -5.53 eV(β), the $C_{17}B$ nanocluster has chemical potentials of -4.85 eV(α) and -5.38 eV(β). Following adsorption, the shift in E_{HOMO} and E_{LUMO} results in μ changes of 16.7%(α), -4.83%(β), 17.1%, -15.7%(α), and 18.4%(β) for CO, NO, and NH_3 adsorption over $C_{17}B$, respectively. For CO, NO, and NH_3 adsorption, respectively, Δμ for $C_{17}N$ is 2.45%(α),0.9%(β), -1.49%, -2.26%(α), and -1.61%(β). The value of μ is greatest when NH_3 is adsorbed over $C_{17}B$, and it is lowest when NO is adsorbed over $C_{17}N$. The stability of a configuration is shown by hardness (η), which changes by -26.3%, -26.3%(α), -26.9%(α), and 11.6%(β) for CO, NO, and NH_3

adsorption over $C_{17}B$ nanocluster, respectively. Δη for $C_{17}N$ is -25.9%(α), 2.42%(β), -26.3%, -26.3%(α), and 11.6%(β) for NH_3 adsorption, CO, and NO, in that order. Whereas softness(S) for $C_{17}B$ rises in the sequence $NH_3/C_{17}B(\alpha) < C_{17}B(\alpha)$ \ $NO/C_{17}B(\alpha)$ \ $CO/C_{17}B(\beta)$, it stays constant for $C_{17}N$ (0.21(α), 0.17(β)) with the exception of NO adsorption, when it drops to 0.18 eV-1. ω, or the tendency of molecules or atoms to absorb electrons, is measured for the $C_{17}B$ and $C_{17}N$ nanoclusters at 3.76(α), 6.95(β), and 5.92(α), 5.19(β), respectively. The alterations for CO, NO, and NH_3 adsorption over the $C_{17}B$ nanocluster are, respectively, 87.2%(α), -11.2%(β), 88.6%, -37.5%(α), and -39.1%(β). In the case of $C_{17}N$, Δω is 5.24%(α), 0.19%(β), 1.86%, -4.22%(α), and -3.66%(β) for the adsorption of CO, NO, and NH_3. In the case of CO and NO adsorption, ω is greater for $C_{17}B$. For $C_{17}N$, ω does not significantly change in any scenario.

Table 4.4: Chemical potential (μ), hardness (η), softness (S) and electrophilicity (ω) for CO, NO and NH_3 adsorbed $C_{17}X$ nanoclusters, respectively.

System	μ (eV)		η (eV)		S $(eV)^{-1}$		ω (eV)	
$C_{17}B$	$-4.85^{(\alpha)}$	$-5.38^{(\beta)}$	$3.08^{(\alpha)}$	$2.07^{(\beta)}$	$0.16^{(\alpha)}$	$0.24^{(\beta)}$	$3.76^{(\alpha)}$	$6.95^{(\beta)}$
$CO/C_{17}B$	$-5.66^{(\alpha)}$	$-5.12^{(\beta)}$	$2.25^{(\alpha)}$	$2.12^{(\beta)}$	$0.22^{(\alpha)}$	$0.24^{(\beta)}$	$7.04^{(\alpha)}$	$6.17^{(\beta)}$
$NO/C_{17}B$	-5.68		2.27		0.22		7.09	
$NH_3/C_{17}B$	$-4.09^{(\alpha)}$	$-4.39^{(\beta)}$	$3.56^{(\alpha)}$	$2.31^{(\beta)}$	$0.14^{(\alpha)}$	$0.22^{(\beta)}$	$2.35^{(\alpha)}$	$4.13^{(\beta)}$
$C_{17}N$	$-5.32^{(\alpha)}$	$-5.53^{(\beta)}$	$2.37^{(\alpha)}$	$2.98^{(\beta)}$	$0.21^{(\alpha)}$	$0.17^{(\beta)}$	$5.92^{(\alpha)}$	$5.19^{(\beta)}$
$CO/C_{17}N$	$-5.44^{(\alpha)}$	$-5.58^{(\beta)}$	$2.37^{(\alpha)}$	$2.99^{(\beta)}$	$0.21^{(\alpha)}$	$0.17^{(\beta)}$	$6.23^{(\alpha)}$	$5.20^{(\beta)}$
$NO/C_{17}N$	-5.73		2.18		0.18		6.03	
$NH_3/C_{17}N$	$-5.19^{(\alpha)}$	$-5.49^{(\beta)}$	$2.38^{(\alpha)}$	$3.01^{(\beta)}$	$0.21^{(\alpha)}$	$0.17^{(\beta)}$	$5.67^{(\alpha)}$	$5.00^{(\beta)}$

4.4. CONCLUSION

We have looked at the doped and pure polyynic cyclo[18]carbons' geometrical, electrical, and sensing characteristics. On pure C_{18}, the harmful gases (CO, NO, and NH_3) exhibit physisorption. Following boron and nitrogen doping, the HOMO-LUMO gap decreases by 8.75% and 29.9%, respectively. When nitrogen is doped, only NO (-1.32 eV) exhibits chemisorption, while the other two gases exhibit physisorption. All three gases (CO, NO, and NH_3) exhibit chemisorption when boron is doped. The adsorption energies are in the following order: CO (-1.41 eV) > NH_3 (-1.81 eV) > NO (-2 eV). The $C_{17}B$ nanocluster is a good candidate

for a conductivity-based (σ-type) sensor for CO and NO gases since any material's sensing response depends on the relative change in electrical conductivity. Given that $C_{17}B$'s calculated recovery time is relatively large (measured in days), it is possible that this material will be employed as a gas molecule remover from certain settings or as a molecular adsorbent for reservoir applications [20]. In contrast, the adsorption energy order for $C_{17}N$ is as follows: CO (-0.15 eV) > NH_3 (-0.25 eV) > NO (-1.32 eV). It suggests that CO and NH_3 adsorption has a quick recovery period, suggesting that the $C_{17}N$ nanocluster might be useful for CO and NH_3 gas sensor applications.

BIBLIOGRAPHY:

[1] S. K. Tiwari, V. Kumar, A. Huczko, R. Oraon, A. De Adhikari and G. C. Nayak, *Crit. Rev. Solid State Mater. Sci.*, 2016, **41**, 257–317.

[2] K. Kaiser, L. M. Scriven, F. Schulz, P. Gawel, L. Gross and H. L. Anderson, *Science (80-.).*, 2019, **365**, 1299–1301.

[3] A. Yadav and N. Sinha, *Mater. Express*, 2022, **12**, 1–33.

[4] K. Timsorn and C. Wongchoosuk, *Mater. Res. Express*, 2020, **7**, 055005.

[5] A. Yadav, *Silicon*, 2023, **15**, 1847–1857.

[6] A. J. Stasyuk, O. A. Stasyuk, M. Solà and A. A. Voityuk, *Chem. Commun.*, 2020, **56**, 352–355.

[7] M. D. Esrafili and H. Janebi, *Mol. Phys.*, 2020, **118**, 1–9.

[8] M. J. Frisch, Trucks, G.W., Schlegel, H.B., Scuseria, G.E., Robb, M.A., Cheeseman, J.R., *Gaussian 09, Revis. A.02, Gaussian, Inc.*, 2016, 1–2.

[9] S. Vadalkar, D. Chodvadiya, N. N. Som, K. N. Vyas, P. K. Jha and B. Chakraborty, *ChemistrySelect*, 2022, **7**, e202103874.

[10] S. K. Jana, D. Chodvadiya, N. N. Som and P. K. Jha, *Diam. Relat. Mater.*, 2022, **129**, 109305.

[11] S. Patel, P. Patel, D. Chodvadiya, N. N. Som and P. K. Jha, *J. Mol. Liq.*, 2022, **352**, 118702.

[12] V. Nagarajan and R. Chandiramouli, *Phosphorus, Sulfur Silicon Relat. Elem.*, 2019, **194**, 25–32.

[13] V. Nagarajan and R. Chandiramouli, *Comput. Theor. Chem.*, 2019, **1150**, 63–70.

[14] F. Opoku, O. Akoto, N. K. Asare-Donkor and A. A. Adimado, *Appl. Surf. Sci.*, 2021, **562**, 150188.

[15] N. R. Sheela, S. Muthu and S. Sampathkrishnan, *Spectrochim. Acta - Part A Mol. Biomol. Spectrosc.*, 2014, **120**, 237–251.

[16] N. A. Tukadiya, S. K. Jana, B. Chakraborty and P. K. Jha, *Surfaces and Interfaces*, 2023, **41**, 1–16.

[17] V. Kumar, A. Bano and D. R. Roy, *ACS Appl. Nano Mater.*, 2021, **4**, 2440–2451.

[18] S. Peng, K. Cho, P. Qi and H. Dai, *Chem. Phys. Lett.*, 2004, **387**, 271–276.

[19] M. A. Hossain, M. R. Hossain, M. K. Hossain, J. I. Khandaker, F. Ahmed, T. Ferdous and M. A. Hossain, *Chem. Phys. Lett.*, 2020, **754**, 137701.

[20] H. Basharnavaz, A. Habibi-Yangjeh and M. Pirhashemi, *Chem. Phys. Lett.*, 2020, **754**, 137676.